

Supplemental Information

Site-1 protease deficiency causes human skeletal dysplasia due to defective inter-organelle protein trafficking

Yuji Kondo^{1‡}, Jianxin Fu^{1,2‡}, Hua Wang³, Christopher Hoover^{1,4}, J. Michael McDaniel¹, Richard Steet⁵, Debabrata Patra⁶, Jianhua Song¹, Laura Pollard⁷, Sara Cathey⁷, Tadayuki Yago¹, Graham Wiley⁸, Susan Macwana⁸, Joel Guthridge⁸, Samuel McGee¹, Shibo Li³, Courtney Griffin¹, Koichi Furukawa⁹, Judith A. James⁸, Changgeng Ruan², Rodger P. McEver^{1,4}, Klaas J. Wierenga^{3*}, Patrick M. Gaffney^{8*}, and Lijun Xia^{1,2,4*}

Correspondence to: Lijun-Xia@omrf.org

This PDF file includes:

Patient information

References

Supplemental Tables 1 to 3

Supplemental Figs. 1 to 7

Patient information

The patient study was approved by the Institutional Review Boards of the University of Oklahoma Health Sciences Center and Oklahoma Medical Research Foundation.

The patient with S1P deficiency is currently 11.5 years of age. She was born following an uncomplicated pregnancy to her gravida 3, para 2 mother and father. Birth weight at term was 2.07 kg, which was small for gestational age at birth. At birth, no obvious abnormalities were identified. Up to 6 months of age, her length and weight were at 5%, after which gain in weight and height slowed down considerably (see growth chart, Supplemental Table 1). At 2 years of age she had bilateral cataract extraction, identified a few months earlier. Attainment of gross motor milestones was delayed, but speech and cognitive development were normal. At age 3 years, she was seen in a pediatric Endocrinology clinic and thought to have Russell-Silver syndrome, but no molecular testing was pursued. Human growth hormone replacement therapy was started but discontinued after 1 year due to limited response. She had elective bilateral inguinal hernia repair at age 3½ years. At age 6 years, she was referred to pediatric orthopedics for back pain. Other than the short stature, she was thought to have an unusual face. Short stature was again observed, and other skeletal findings were pectus carinatum, kyphosis, and waddling gait. Radiology done at that time revealed spondylo-epiphyseal dysplasia with associated kyphosis. She was referred to Medical Genetics. A SNP (single nucleotide polymorphism) array revealed a heterozygous duplication on chr19q13.42 (genomic coordinates: chr19:54,659,105-55,909,948 x3, hg19), found to be maternally inherited, and therefore assessed as a likely harmless copy number variant. *COL2A1* (MIM (Mendelian inheritance in man database number) 120140) sequencing was performed and found to be normal. At age 8 years, she was found to have markedly elevated plasma levels of various lysosomal enzymes (β -galactosidase, β -

mannosidase, α -mannosidase, β -glucuronidase, α -glucosaminidase, and β -hexosaminidase), which was confirmed on repeat testing, while urinary glycosaminoglycans were normal. Deficient activity of UDP-N-acetylglucosamine:lysosomal-enzyme N-acetylglucosamine-1-phosphotransferase (GlcNAc-phosphotransferase; EC 2.7.8.17) was suspected. However, Sanger sequencing revealed no predicted pathogenic variants in *GNPTAB* (MIM 607840) and *GNPTG* (MIM 607838). Through whole exome sequencing, bi-allelic variants in *MBTPSI*, which encodes site-1 protease (S1P), were identified. The paternal variant was a nucleotide duplication (NM_003791.3: c.285dupT) in exon 3, predicted to create a nonsense change (p.D96X) (Fig. 1C). The maternal variant was a nucleotide substitution (NM_003791.3: c.1094A>G) in exon 9, predicted to result in a missense variant substituting aspartic acid for glycine (p.D365G). At age 9 years, a complete metabolic panel (including alkaline phosphatase) was normal; serum calcium was also normal, and parathyroid hormone was intact. At age 10 years, complete blood count was normal, and biochemical studies done as part of a bone health evaluation revealed normal bone-specific alkaline phosphatase (56.4 μ g/L, normal 47.9-150.8), elevated serum N-telopeptide (44.4, normal 6.2-19.0), elevated urine N-telopeptide/creatinine ratio (907, normal in Tanner Stage II Female 193-514), and elevated osteocalcin (58.0 ng/mL, normal in pre-menopausal women: 4.9-30.9). DXA scan revealed a z-score of -4.5 at total body less head (TBLH), and a z-score of -3.3 at anterior-posterior (AP) spine. Even after correcting for her significant short stature, this is low. Vitamin D studies were normal. Echocardiogram at age 10½ years was normal. Radiographs done at 11½ years of age revealed stable complete anterolisthesis of vertebra L5 on S1 and bilateral shortening of the femoral necks with irregular and dysplastic appearance of the femoral and proximal tibial epiphyses. Fibula are gracile with valgus bowing.

She had dysmorphic facial features, with prominent forehead, prominent cheekbones, and large ears.

For comparison, we also identified a patient with a mutation in *MBTPS2* (the membrane-bound transcription factor peptidase, site 2, S2P). S2P functions sequentially with S1P to cleave transmembrane transcription factors in response to ER stress or decreased sterol metabolites, important for regulating lipid biosynthesis and ER stress (1, 2). This patient has a hemizygous variant in *MBTPS2* (c.1523 A>G, p.N508S, X-linked), inherited from his mother. This patient has short stature, developmental delay, seizures, photophobia, ichthyosis follicularis, and reduced body hair. The p.N508S variant in *MBTPS2* has been reported previously, with hemizygous males presented with keratosis follicularis spinulosa decalvans (KFSD) (3).

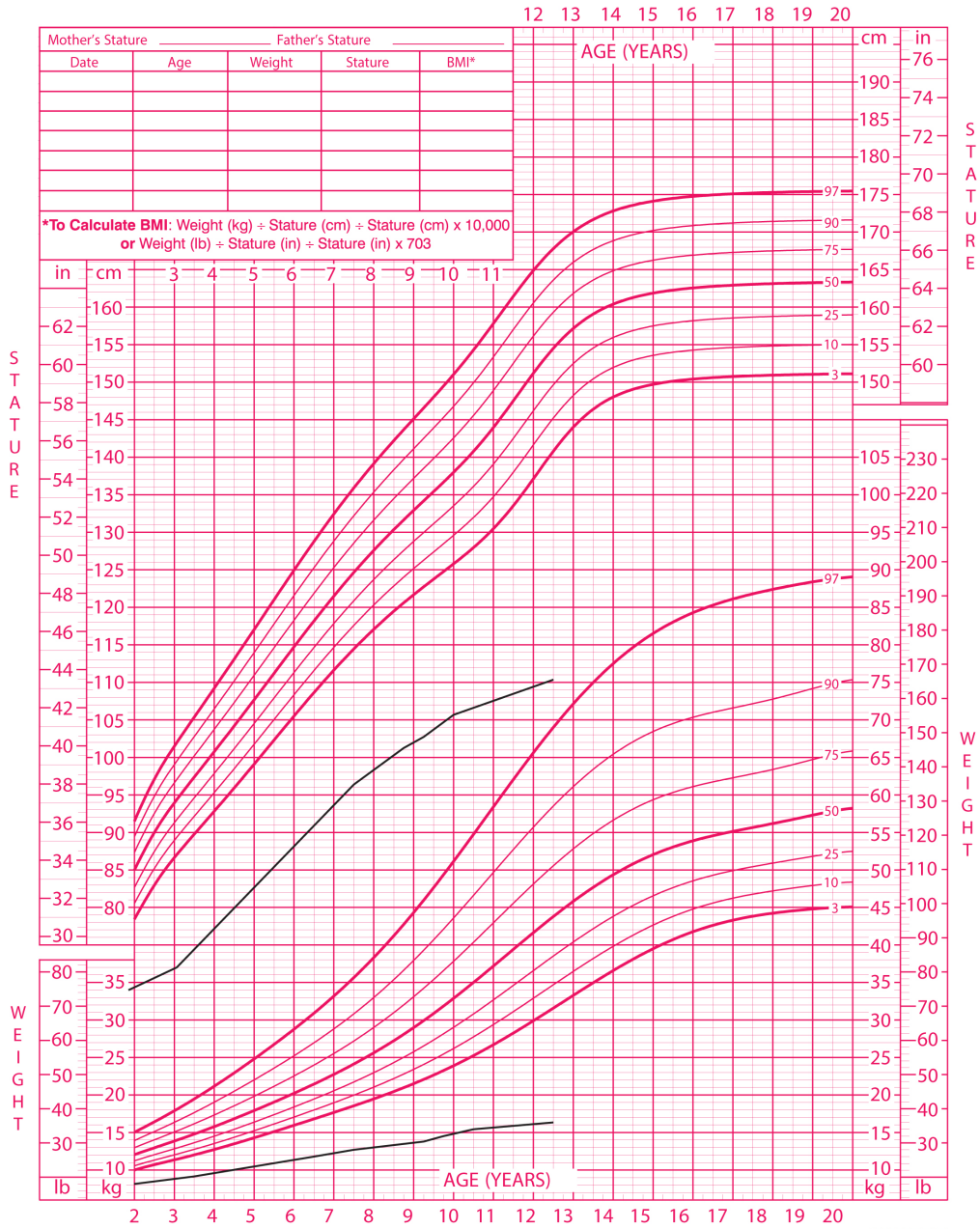
References:

1. Brown, MS,Goldstein, JL. The SREBP pathway: regulation of cholesterol metabolism by proteolysis of a membrane-bound transcription factor. *Cell*. 1997;89(3):331-340.
2. Yang, J, Goldstein, JL, Hammer, RE, Moon, YA, Brown, MS,Horton, JD. Decreased lipid synthesis in livers of mice with disrupted Site-1 protease gene. *Proc Natl Acad Sci U S A*. 2001;98(24):13607-13612.
3. Lindert, U, et al. MBTPS2 mutations cause defective regulated intramembrane proteolysis in X-linked osteogenesis imperfecta. *Nat Commun*. 2016;7(11920).

2 to 20 years: Girls
Stature -for-age and Weight-for-age percentiles

NAME _____

RECORD # _____



Published May 30, 2000 (modified 11/21/00).
SOURCE: Developed by the National Center for Health Statistics in collaboration with
the National Center for Chronic Disease Prevention and Health Promotion (2000).
<http://www.cdc.gov/growthcharts>



Supplemental Table 1. The growth chart of the S1P-deficient patient, which includes data on body length and weight of the patient (black lines) relative to the percentiles for healthy girls up to 20 years of age.

	S1P deficiency	Mucopolipidosis II/III	KFSD syndrome	OI syndrome
Mutated gene	<i>MBTPS1</i>	<i>GNPTAB</i>	<i>MBTPS2</i> (p.N508S)	<i>MBTPS2</i> (p.N459S and p.L505F)
Affected protein	S1P	GPT	S2P	S2P
Reduced cognition	no	yes	yes	no
Short stature	yes	yes	yes	yes
Cataract	yes	no	no	n/a
Visual (photophobia)	no	no	yes	no
Blue sclerae	no	no	no	yes
Alopecia	no	no	normal scalp hair, reduced eyebrow and body hair	no
Ichthyosis follicularis	no	no	yes	no
Valvular cardiac defects	no	yes	n/a	n/a
Inguinal hernia	yes	yes	yes	no
Bone dysplasia	yes	yes	yes	yes
Blood lipids	yes (modest)	no	n/a	n/a
Elevated blood lysosome enzymes	yes	yes	no	n/a
Elevated urine N-telopeptide/creatinine ratio	yes	yes	no	no
Affected organelle	lysosome and ER	lysosome	ER	ER
Cellular defects	defective functions of lysosome and ER	defective function of lysosome	defective function of ER	defective functions of ER and collagen crosslinks

Supplemental Table 2. Comparison of the *MBTPS1* mutation-caused syndrome with ML-II/III, and *MBTPS2* mutation-caused syndromes. ML-II/ III caused by genetic mutation in *GNPTAB* leads to skeletal dysplasia due to bone absorption and defective lysosomal functions. *MBTPS1*-encoded S1P and *MBTPS2*-encoded S2P are localized in the Golgi membrane. They sequentially cleave transcription factors to regulate ER stress or cholesterol synthesis. Although patients with pathogenic *MBTPS2* variants have diverse clinical presentations (osteogenesis

imperfecta, OI syndrome, X-linked; keratosis follicularis spinulosa decalvans, KFSD syndrome, X-linked) (3), they all exhibit various degrees of skeletal malformation, which are primarily caused by defective ER functions. By contrast, the patient in this study with a syndrome caused by genetic mutation in *MBTPSI* shows skeletal dysplasia due to compound defects of lysosomes and ER.

<i>Hprt</i> :	forward primer, 5'- CCTGCTGGATTACATCAAAGCACTG -3'
	reverse primer, 5'- GTCAAGGGCATATCCTACAACAAAC -3'
<i>Mbtps1</i> :	forward primer, 5'- TCCAATTGCTTGGATGACAG -3'
	reverse primer, 5'- TCCAGAACCTTGGAGTACCG -3'
<i>Dhcr7</i> :	forward primer, 5'- ACGCTGCAGGGTCTGTACTT -3'
	reverse primer, 5'- ACAGGTCCTTCTGGTGGTTG -3'
<i>Sec23a</i> :	forward primer, 5'- ACCAAAGACATGCATGGACA -3'
	reverse primer, 5'- CACAAACTGGATTGCACCAC -3'
<i>Coll1</i> :	forward primer, 5'- AGCCAGCAGATCGAGAACAT -3'
	reverse primer, 5'- TCTTGTCTTGGGGTTCTTG -3'
<i>Hspa5</i> :	forward primer, 5'- TAGCGTATGGTGCTGCTGTC -3'
	reverse primer, 5'- TTTGTCAAGGGTCTTTCACC -3'
<i>Ddit3</i> :	forward primer, 5'- CAGAACCAGCAGAGGTCACA -3'
	reverse primer, 5'- TCACCATTCCGGTCAATCAGA -3'
<i>Runx2</i> :	forward primer, 5'- GACGAGGCAAGAGTTCACC -3'
	reverse primer, 5'- GCCTGGGGTCTGTAATCTGA -3'
<i>Col2a1</i> :	forward primer, 5'- CAGTTGGGAGTAATGCAAG -3'
	reverse primer, 5'- GCCTGGATAACCTCTGTG -3'
<i>Coll10a1</i> :	forward primer, 5'- AGGAATGCCTGTGTCTGCTT -3'
	reverse primer, 5'- ACAGGCCTACCCAAACATGA -3'
<i>Trappc2</i> :	forward primer, 5'- GGAAGGCAGAATCCAAAGACG -3'
	reverse primer, 5'- ATGCCGACACAAACCACTCG -3'
<i>Mia3</i> :	forward primer, 5'- CCTTGAGGCAGAAAGTGGAG -3'
	reverse primer, 5'- CATGGGTAGCGATCTGGTTT -3'
<i>Serpinh1</i> :	forward primer, 5'- AGCAGCAAGCAGCACTACAA -3'
	reverse primer, 5'- AGGACCGAGTCACCATGAAG -3'

Supplemental Table 3. qPCR primers

Supplemental Figures

Supplementary Fig. 1

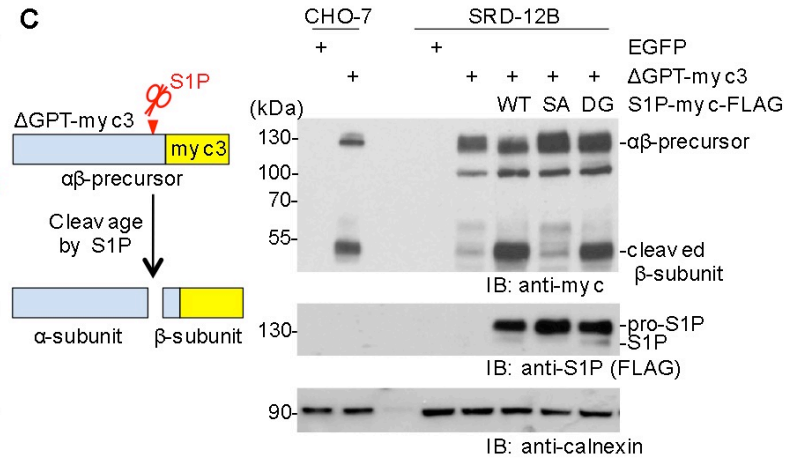
A



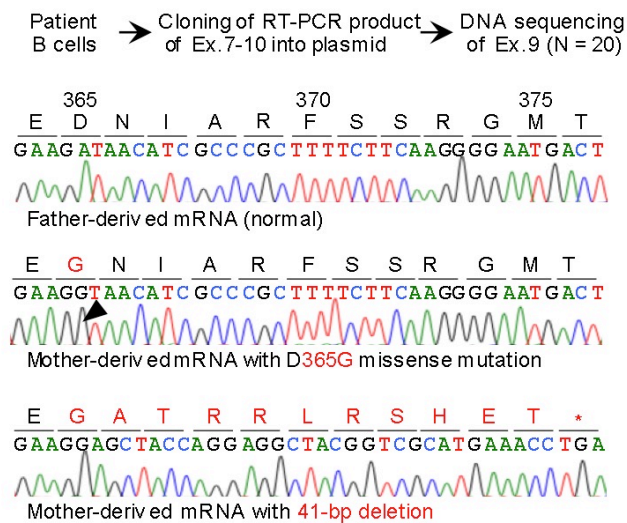
B



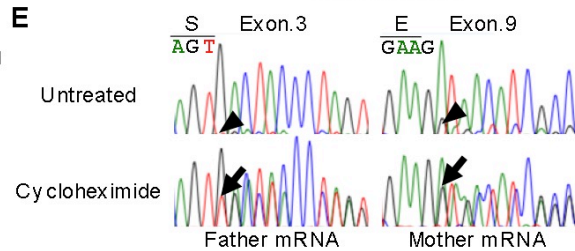
C



D



E



F

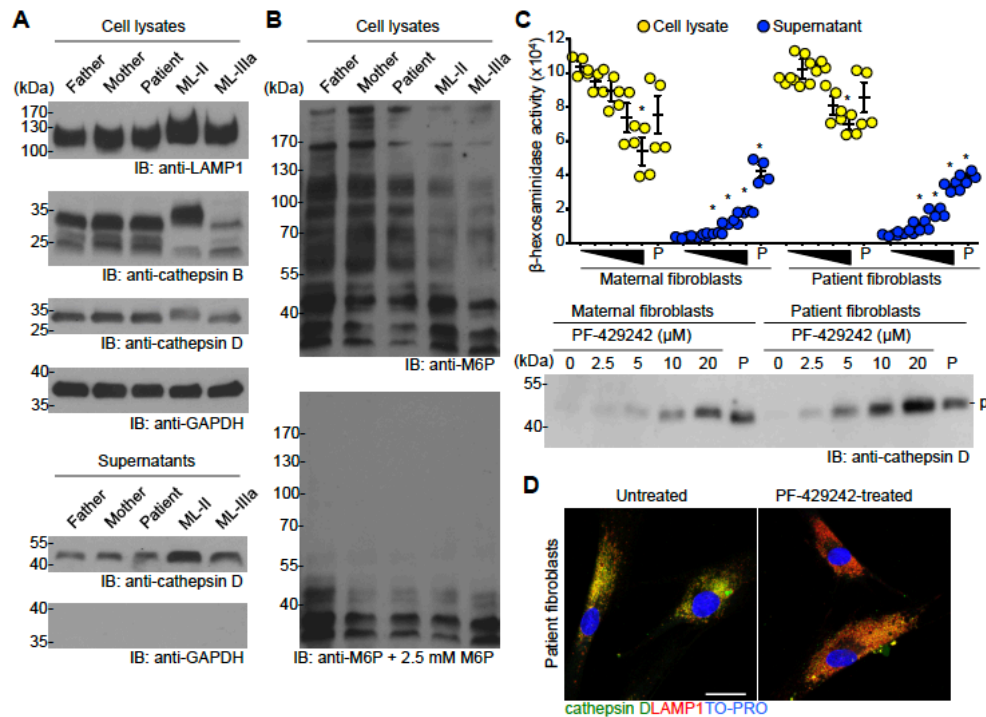
Types of variants	% of each variant expressed	% each transcript relative to control
Paternal D96X	55% (11/20)	11% (0.2 x 55%), non-functional
Maternal D365G	5% (1/20)	1% (0.2 x 5%), functional
Maternal 41-bp deletion	40% (8/20)	8% (0.2 x 40%), non-functional

Supplemental Figure 1. Identification of *MBTPS1* compound heterozygote variants in a pediatric patient clinically diagnosed as mucopolysaccharidosis III and recombinant S1P expressed

by CHO cells transfected with *MBTPSI* cDNA with the maternal mutation exhibits normal protease activity. (A) stable complete anterolisthesis of vertebra L5 on S1 with spondylo-epiphyseal dysplasia (I, back; II, side), gracile fibula with valgus bowing of the tibia due to defective endochondral ossification (III), and brachydactyly (IV). (B) Predicted catalytic domain of human S1P. Red, p.D365 site. Green, catalytic triad. The p.D365 is far from catalytic triad. (C) Western blotting of lysates from control WT CHO cells (CHO-7) and S1P-deficient CHO cells (SRD-12B) transfected with the indicated constructs. EGFP construct, negative control. Δ GPT-myc3, a construct encoding myc3-tagged GPT reporter. WT, normal non-mutated *MBTPSI* cDNA construct with C-terminal myc-FLAG tag. SA, *MBTPSI* cDNA construct with the catalytic-defective mutation S414A with C-terminal myc-FLAG tag. DG, *MBTPSI* cDNA with the maternal mutation D365G with C-terminal myc-FLAG tag. Precursor and cleaved forms of the reporter substrate were detected in WT CHO-7 cells but not in S1P-defective CHO mutant SRD-12B cells. However, cleaved reporter substrate was detected in SRD-12B cells after co-transfection with either WT or S1P^{D365G} (DG) but not with catalytically inactive S1P^{S414A} (SA). (D) DNA sequences of three forms of cloned exon 9 of the *MBTPSI* cDNA expressed in patient-derived immortalized B cells. Of the expressed transcripts, 55% are father-derived (top), 5% and 40% are mother-derived with a missense mutation (D365G, middle) and a 41-bp deletion (bottom), respectively. (E) DNA sequences of exon 3 and exon 9 of *MBTPSI* cDNA expressed in paternal or maternal immortalized B cells after treatment with the nonsense mediated mRNA decay (NMD) inhibitor cycloheximide for 6 hrs. Compared with expression levels in untreated cells, mutant transcripts are relatively increased by cycloheximide treatment, indicating that mutant transcripts are unstable due to the NMD quality control system. (F) Percentage of three different *MBTPSI* variants expression in the patient cells. Cloned patient *MBTPSI* exon 9

cDNAs were sequenced to quantify each transcript. Given that 20% total *MBTPSI* expression in the patient (Figure 1E), ~1% functional *MBTPSI* with p.D365G is expressed in the patient. All data are from three independent experiments. All results are representative of three independent experiments.

Supplementary Fig. 2.

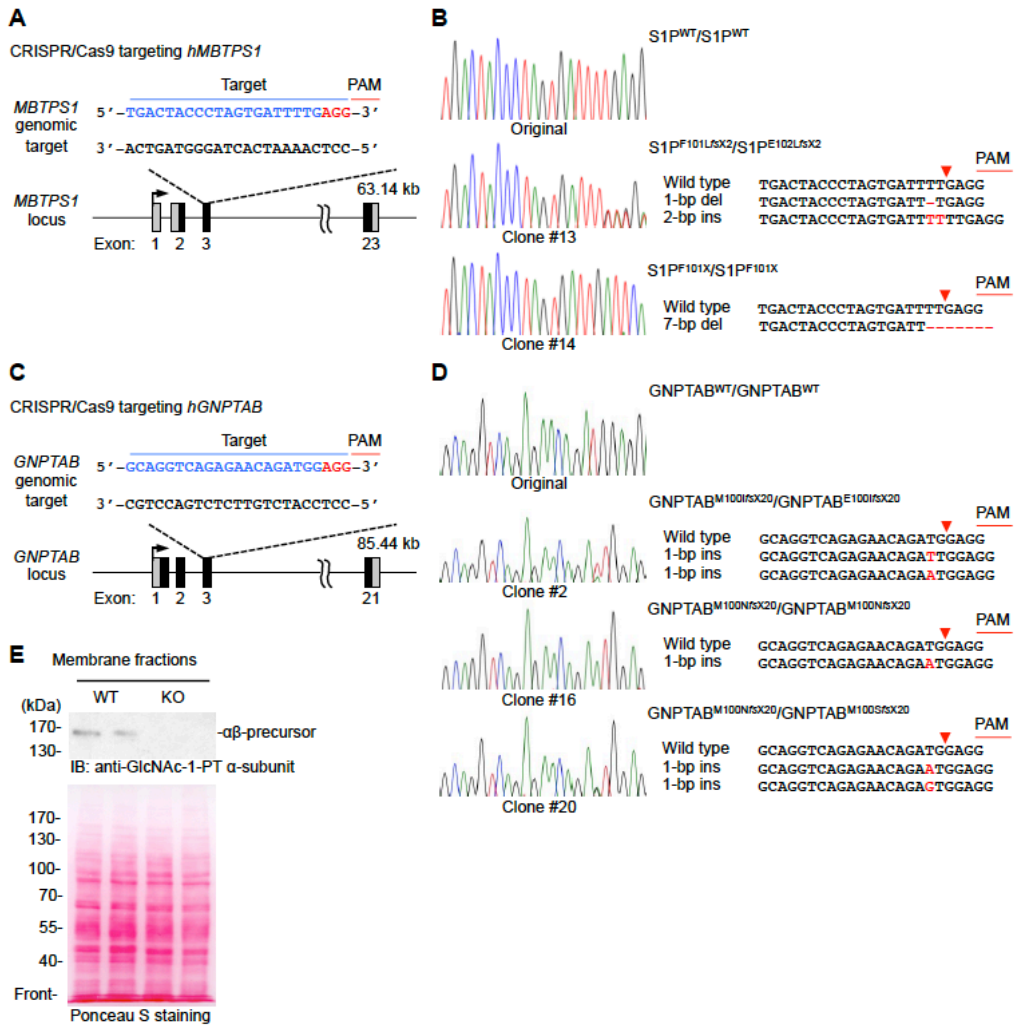


Supplemental Figure 2. Patient fibroblasts do not have mucopolidosis phenotypes. (A)

Western blotting of lysosomal proteins in lysates and culture supernatants from fibroblasts. Anti-GAPDH, loading control. ML-II and ML-IIIa lysates or supernatants, positive controls. Unlike in ML-II and ML-IIIa cells, LAMP1, cathepsin B and cathepsin D were detected in lysates of patient cells at levels similar to those in parental cells. Excessive secretion of cathepsin D into the culture supernatant was not observed in patient cells. **(B)** Western blotting of M6P modification in primary fibroblast lysates (top). Incubation of the same membrane with free M6P as a competitive inhibitor abolishes the anti-M6P binding, confirming the specificity of anti-M6P scFv (bottom). **(C)** β -hexosaminidase activity in lysates or supernatants (top) and western blotting of cathepsin D in supernatant (bottom) from maternal and patient-derived fibroblasts treated with S1P inhibitor PF-429242 (48 hrs) as indicated. P, NH₄Cl treated. Data represent means \pm SEM; n = 34. * $P < 0.05$. **(D)** Representative immunofluorescence images of patient-derived fibroblasts treated with S1P inhibitor PF-429242 (48 hrs). Like ML-II and ML-IIIa cells,

S1P inhibitor-treated patient-derived fibroblasts displayed mucopolipidosis phenotypes, indicating residual S1P activity is sufficient enough for patient fibroblasts to maintain proper lysosomal functions at least in resting states. Cathepsin D, lysosome enzyme; LAMP1, lysosome marker. TO-PRO, nuclear counter-staining. Scale bar, 10 μm .

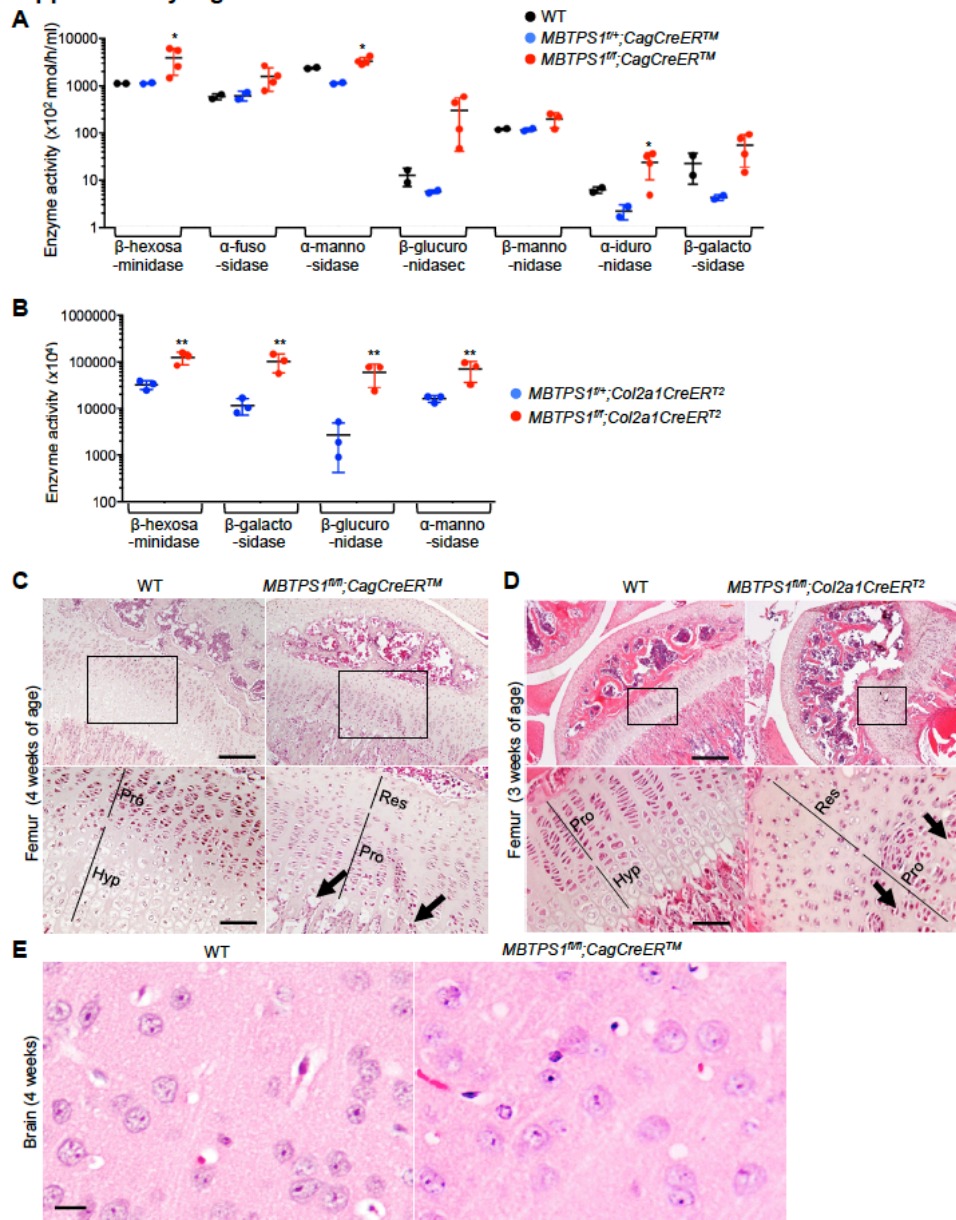
Supplementary Fig. 3.



Supplemental Figure 3. Generation of S1P-deficient and GPT-deficient (KO) cells by CRISPR/Cas9-mediated gene editing. (A) Targeting strategy to generate S1P-KO cells. A short guide RNA (sgRNA) was designed to target exon 3 of human *MBTPS1*. (B) Direct DNA sequences of edited genomes from S1P-KO clones. Clones #13 and #14 have frameshift-mediated nonsense mutations (red arrowheads) in exon 3 of *MBTPS1*, resulting in gene disruption. (C) Targeting strategy to generate GPT-KO cells. An sgRNA was designed to target exon 3 of human *GNPTAB*. (D) Direct DNA sequences of edited genomes from GPT-KO clones. Clones #2, #16, and #20 have frameshift-mediated nonsense mutations (red arrowheads) in exon

3 of *GNPTAB*, resulting in gene disruption. (E) Western blotting of membrane fractions of different GPT-KO cell clones to validate the loss of GlcNAc-1-phosphotransferase $\alpha\beta$ ($\alpha\beta$ -precursor). Ponceau S staining was used as a loading control. The results are representative of two independent experiments.

Supplementary Fig. 4.



Supplemental Figure 4. $MBTPS1^{fl/fl};CagCreER^{TM}$ mice and $MBTPS1^{fl/fl};Col2a1CreER^{T2}$

mice have elevated circulating lysosomal enzymes and defective development of the

hypertrophic chondrocyte layer of cartilage tissues. (A and B) Activities of lysosomal

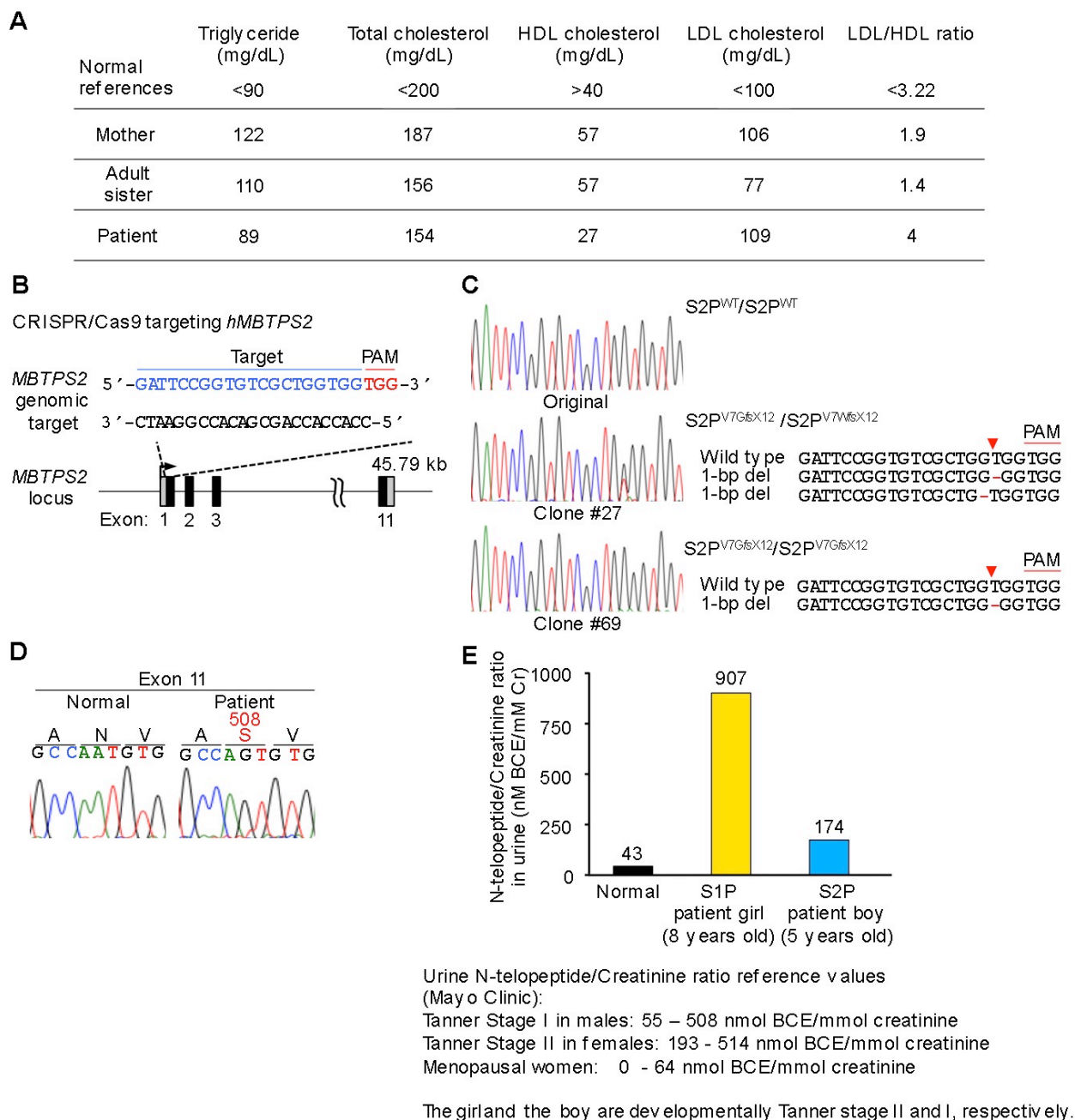
enzymes in serum were analysed from WT and various $MBTPS1$ mutant mice. Highly elevated

levels of the lysosomal enzymes were detected in serum from $MBTPS1$ mutant mice including

the chondrocyte-specific inducible S1P-KO mice at embryonic day 18 (E18.5) relative to WT

controls. Each dot represents a single mouse. [Data represent means \$\pm\$ SD; n = 3 - 4. * \$P < 0.05\$, ** \$P < 0.01\$.](#) (C and D) Femur sections of WT and various *MBTPSI* mutant mice (3-4 weeks of age) stained with haematoxylin and eosin (H&E). Res, resting chondrocyte layer; Pro, proliferating chondrocyte layer; Hyp, hypertrophic chondrocyte layer. Arrows indicate lack of hypertrophic chondrocytes. Skeletal dysplasia is caused by the disrupted growth plate where hypertrophic chondrocytes are lacking and therefore no longitudinal growth. Scale bar, 200 μ m (top), 100 μ m (bottom). (E) H&E-stained sections of WT and *MBTPSI^{ff};CagCreERTM* brain (4 weeks of age). Scale bar, 10 μ m. Unlike reported GPT-deficient mice, S1P-deficient mice do not have inclusion body in neuronal cells, suggesting residual GPT activity in S1P-deficient neurons is possibly due to S1P-independent activation mechanism of GPT.

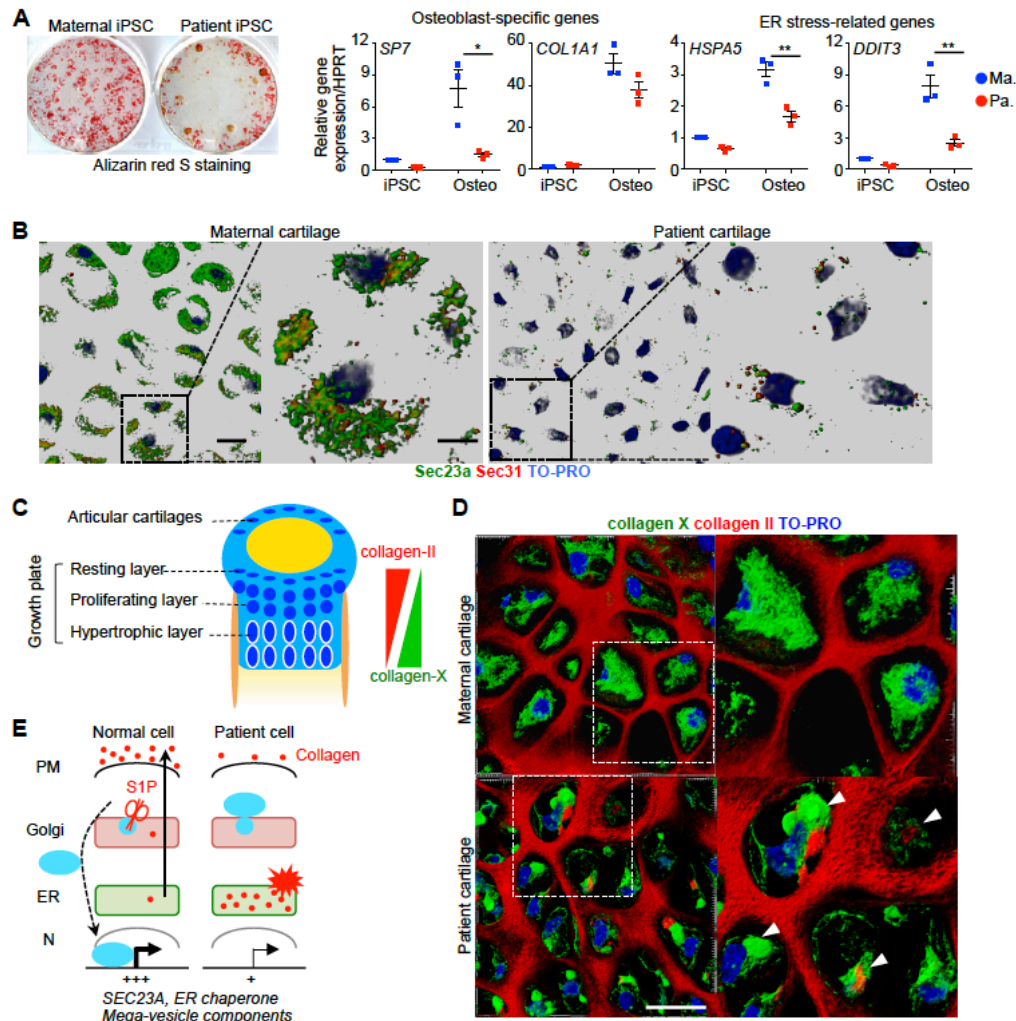
Supplementary Fig. 5.



Supplemental Figure 5. Characterization of S2P-deficient patient and cells. (A) Serum levels of triacylglyceride, total cholesterol, high density lipoprotein (HDL) and low density lipoprotein (LDL) were analysed. Slightly low level of serum HDL (27 mg/dL) in the patient compared with in mother and her sister (57 mg/dL). (B) Targeting strategy to generate S2P-KO

Saos2 cells. A sgRNA was designed targeting exon 1 of human *MBTPS2*. (C) Direct DNA sequences of edited genomes from S2P-KO clones. Clones #27 and #69 have frameshift-mediated nonsense mutations (red arrowheads) in exon 1 of *MBTPS2*, resulting in gene disruption. (D) Sequences of Exon 11 of *MBTPS2* from cDNA isolated from the leukocytes of a S2P patient. (E) Urine N-telopeptide/Creatinine ratio, a urine biomarker for active bone matrix degradation mediated by collagenases. The boy patient's mother was enrolled in this study as a normal control. As expected, higher N-telopeptide/Creatinine ratio was found in the S1P patient due to elevated secretion of collagenases but not in the S2P patient, indicating contribution of lysosomal defect on skeletal defects in the S1P patient but not in the S2P patient.

Supplementary Fig. 6.



Supplemental Figure 6. Generation and characterization of patient and parent fibroblast-

derived iPSCs and iPSC-derived teratomas. (A) Parent and patient-derived iPSCs were

cultured in osteogenic medium for 2 weeks, and then stained with Alizarin red S for

mineralization during osteogenesis (left). Expression profiles of osteoblast-specific genes and ER

stress-related genes in mother (Ma.)-derived and patient (Pa.)-derived iPSCs were analysed by

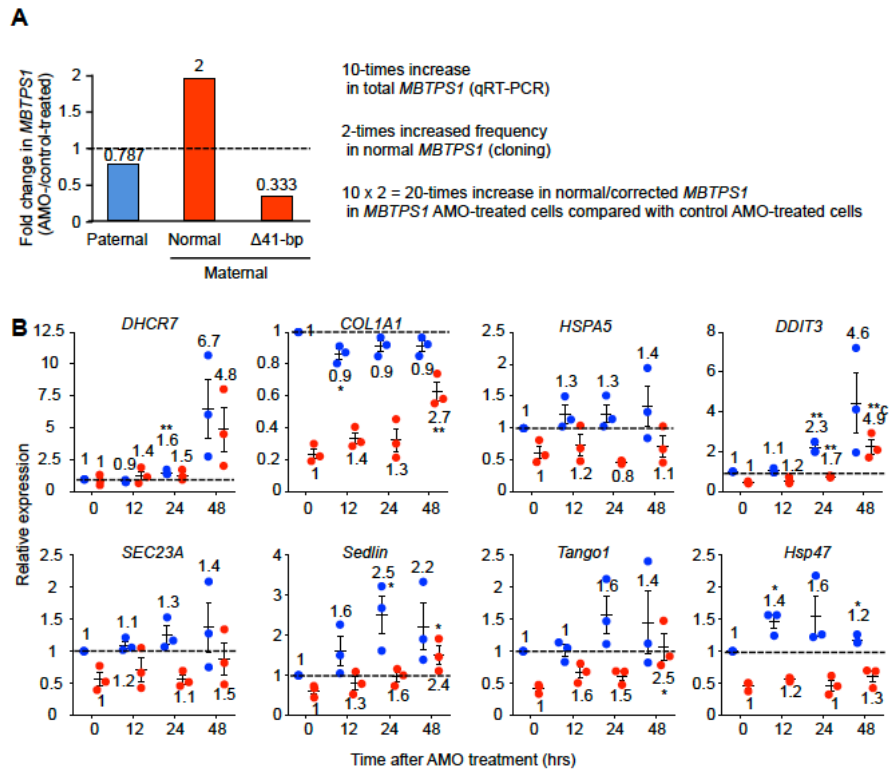
quantitative RT-PCR after culture in osteogenic medium for 2 weeks (right). Defective

derivation of osteoblasts from patient-iPSCs compared with maternal iPSCs. Impaired induction

of osteoblast-lineage genes and UPR in the patient cells after osteogenic induction. [Data](#)

represent means \pm SEM; n = 3. * P < 0.05, ** P < 0.01. (B) Confocal images of immunofluorescence staining of Sec23a and Sec31 in the COP-II vesicles in cartilage in teratomas. Scale bar, 10 μ m (left), 5 μ m (right). As is the case with reported BBF2H7-deficient mice, dramatically reduced Sec23a was found in cartilages in patient teratomas compared with maternal cartilages, indicating impaired formation of COP-II vesicles in patient chondrocytes. (C) Schematic illustration of chondrocytic layers in the growth plate of a long bone. Collagen II is expressed in resting and proliferating chondrocytes, whereas collagen X is predominantly expressed in hypertrophic chondrocytes. (D) Maternal-derived and patient-derived teratomas were stained with antibodies against collagen II and collagen X. Arrowheads indicate densely-stained aggregate-like structures. Scale bar, 20 μ m. The results are representative of three independent experiments. (E) Models of defective collagen trafficking in S1P-deficient cells. Red dots, collagen I/II. In normal cells, accumulation of collagen in ER during development causes physiological ER stress and following proteolytic activation of BBF2H7 by S1P and S2P. Then, cytoplasmic BBF2H7 translocates into nucleus to induce gene expression of Sec23a, ER chaperons, mega vesicle components to release collagen in ER to extracellular space. By contrast, proteolytic activation of BBF2H7 is impaired in the patient, thus the patient cells are compromised with cytotoxic prolong ER stress caused by ER accumulation of collagen.

Supplementary Fig. 7.



Supplemental Figure 7. Blocking the pathogenic splicing using AMO improves defective cellular functions of patient fibroblasts. (A) Summary of the DNA sequences of three forms of cloned exon 9 of *MBTPS1* cDNA expressed in patient fibroblasts treated with AMO. Compared with control oligo treatment, AMO treatment increased 2-fold in correctly spliced transcript. Given that 10-fold increase of total *MBTPS1* expression (Figure 6B, left), the absolute maternal transcript with a missense mutation (p.D365G) is increased 20-fold compared with control oligo-treated cells. (B) The mRNA expression of an SREBP-regulated gene (*DHCR7*), collagen I (*COL1A1*), ER stress-related genes (*HSPA5* and *DDIT3*), the secretory component (*SEC23A*) and mega vesicle components (*Sedlin*, *Tango1* and *Hsp47*) were analysed by quantitative RT-PCR after treatment with AMO. Blue, mother; red, the patient. The number indicates the fold change relative to time 0. [Data represent means \$\pm\$ SEM; n = 3. * \$P < 0.05\$, ** \$P < 0.01\$.](#)